

Characterization of the Teledyne CHROMA HgCdTe Detector for Imaging Spectrometers

Peter Sullivan, Michael Bernas, Elliott Liggett, Michael Eastwood, Robert Green
Jet Propulsion Laboratory, California Institute of Technology
4800 Oak Grove Dr Pasadena, CA 91109
818-354-4207
Peter.Sullivan@jpl.nasa.gov

Abstract—Imaging spectroscopy places high demands upon detector performance. The dynamic range, linearity, and sensitivity must be maintained at high frame rates, and artifacts must be minimized across large focal plane array (FPA) formats. In this contribution, we discuss the Teledyne CHROMA HgCdTe FPA in the context of imaging spectrometer applications. The FPA was characterized in a laboratory thermal-vacuum chamber that allowed the read noise, dark current, well capacity, linearity, and crosstalk to be measured. Results are presented across a range of operating temperatures and pixel clock rates. Additionally, the outcomes of radiation testing to 100 krad TID are discussed. The results of these characterizations are critical to the designs and performance predictions of future imaging spectrometers utilizing the HgCdTe CHROMA FPA.

Keywords: Imaging Spectroscopy, Hyperspectral imaging, HgCdTe detectors, IR Focal Plane Arrays

TABLE OF CONTENTS

1. INTRODUCTION.....	1
2. RADIATION TESTING.....	1
3. POST-RADIATION TEST METHODOLOGY.....	2
4. DATA.....	3
5. ANALYSIS.....	3
6. RESULTS AND DISCUSSION.....	4
7. CONCLUSIONS AND FUTURE WORK.....	6
ACKNOWLEDGMENTS.....	7
REFERENCES.....	7

1. INTRODUCTION

In a pushbroom imaging spectrometer, a two-dimensional detector array is used to simultaneously record spatial information in one dimension and spectral information in the other dimension. If an imaging spectrometer is mounted to a moving vehicle or a scanning platform, a 3-dimensional image cube is constructed with a full spectrum for each field angle. Imaging spectrometers that measure reflected sunlight typically operate from visible to shortwave infrared (SWIR), while those measuring thermal emission will operate out to longwave infrared (LWIR), to detect the molecular features unique to the chemical composition of the scene.

Since spatial and spectral features can rapidly vary across a scene, the FPA must accurately respond to these variations. In addition to the imaging and dispersing optics, the FPA is an important consideration in the spectral response function (SRF) and the spatial, or cross-track, response function (CRF) of an instrument.

The Teledyne TCM 6604-B, or CHROMA, FPA [1] is a new family of devices designed for imaging spectroscopy and other analytic applications. It utilizes a 3.3V CMOS process and has 30 μm pixels. The full well capacity of the pixel amplifier can have one of several values; the devices in this paper are constructed for 1 Me⁻. Programmable registers set the values of digital-to-analog converters (DACs) and timing parameters to bias and control its operation. The readout integrated circuit (ROIC) is hybridized to a photosensitive material, typically Si (for visible to near-infrared applications) or HgCdTe (for sensitivity into SWIR through LWIR channels).

For spaceborne instruments, the FPA must also function under ionizing radiation. The ROIC must not latch up from single events, and performance must not degrade with total ionizing dose (TID). Section 2 describes our testing of an FPA irradiated to 100 krad TID and subjected to a planetary protection bakeout.

2. RADIATION TESTING

The CHROMA FPA was irradiated with a Cobalt-60 source. The TID was delivered in 11 doses of roughly logarithmic steps using a fluence of 1 to 5 rad/s. We tested the CHROMA FPA before, during, and after the doses with measurements of the dark current, dark noise, internal FPA test points, sweeps of internal digital-to-analog converters (DACs), and basic responsivity. The CHROMA was operating during irradiation, which allows for in-situ detection of possible latch-up, startup sequence mishaps, and data corruption in the device.

After reaching 100 krad TID, the CHROMA was placed in a dry heat microbial reduction (DMHR) bakeout at 125°C for 5 hours at a pressure <1 Torr. This temperature and duration is based on previous mission planetary protection procedures, which are necessary for an instrument to sent to areas in the Solar System designated as a region of astrobiological interest. However, this bakeout also serves to anneal radiation damage, as data taken after the bakeout shows.

ROIC DACs and Current Consumption

In order to assess changes to the FPA from radiation, we carefully measured the current drawn by the CHROMA's power supplies. Besides looking at normal idle current, we stepped the internal DACs across through their full ranges and recorded changes in total current consumption. Combining these data can reveal any change in DAC step size, missing DAC bits, and dynamic range. Several of the DACs exhibited missing codes after 100 krad TID. However, in all cases, the annealing process brought behavior back to pre-radiated performance.

TID [krad]	0	40	100	Post-Bake
Power Dissipation [mW]	261.1	261.1	355.5	296.0
Dark Level [DN]	1150	1175	2620	940
Dark Noise [DN]	25.64	23.95	88.53	23.58
Correct Startup	Yes	Yes	Yes	Yes
Register Integrity	Yes	Yes	Yes	Yes
Latchup Events	N/A	None	None	None

Table 1: FPA performance measured at specific exposure levels. After the DHMR bakeout, many aspects of FPA performance returned to near-initial values. The pixel clock is 10 MHz in all cases, and the conversion gain is approximately $25 e^-/\text{DN}$.

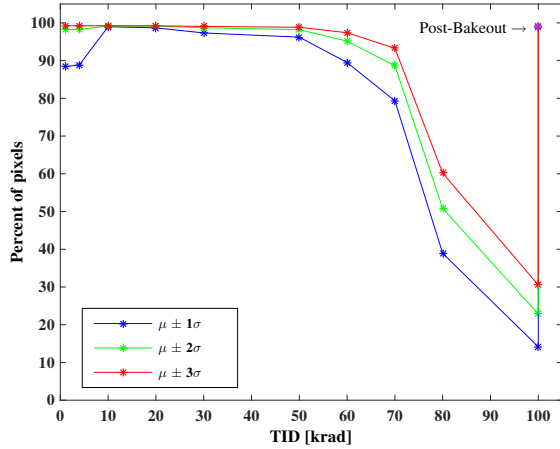


Figure 1: Percentage of pixels contained within specified noise level a function of TID. Both the mean μ and standard deviation σ refer to the pre-radiation values.

Dark noise per pixel

Figure 1 shows how the number of pixels with dark noise measurements remaining within 1, 2, or 3 σ of the original mean noise decreases with TID. Radiation does not effect all pixels uniformly, but those with degraded performance seem to return to the original noise distribution after the bakeout.

Radiation Test Results

Despite the degradation in DAC performance, the CHROMA has shown basic utility at all levels of exposure tested. Table 1 summarizes the results. In-situ reboots were always successful, zero latch up events were observed, and data registers did not show any corruption. For missions with less than 40 krad TID, device radiation characterization and annealing may not be necessary. On missions with greater lifetime exposure, in-mission annealing should be considered. Our successful planetary protection bakeout process also demonstrates the ruggedness of the ROIC, hybridization of the HgCdTe, and packaging. Overall, the radiation test should serve as a useful point of confidence for missions requiring performance with high lifetime dosage levels.

3. POST-RADIATION TEST METHODOLOGY

After radiation testing, we characterized a new CHROMA FPA in a laboratory thermal-vacuum chamber with quieter

electronics.

Using the photon transfer method [2], we examined the relationship between the signal and its variance to reveal the gain, read noise, and well capacity of a FPA. Our analysis of the data is further detailed in Section 5.

In addition to the photon transfer measurements at 150 K, we took additional data at 180 K and 200 K to measure the dark current. We also monitored the light reaching the FPA with an independent reference diode to assess the linearity of the CHROMA FPA.

Electronics

The CHROMA FPA has analog outputs, so it is crucial to accurately convert its output to a digital format. We employ a low-noise, 16-bit analog-to-digital converter (ADC) housed in its own chassis outside the vacuum chamber. Between the FPA and the ADC, a low-noise amplifier (LNA) drives the analog signal out of the vacuum chamber. The LNA provides a high-impedance input, and the distance from the FPA to the LNA is minimized to reduce the capacitive load on the FPA's outputs. The conversion gain from the FPA output to the ADC output is approximately $46 \mu\text{V}$ per digital number (DN).

In order to accurately measure the read noise of the CHROMA, we must verify that the external electronics do not dominate the FPA's noise. With the FPA outputs connected to an internal reference, we measured the electronic noise of this fixed voltage with the full noise bandwidth of our signal chain. Shown in Table 2, the electronic noise ranges from 3.6 to 4.0 DN. This gives an effective number of bits (ENOB) of at least 14 and a signal-to-noise ratio (SNR) greater than 84.3.

We also noted the current draw of the electronics without the FPA so that we could later measure the current with the FPA operating and infer the power dissipation of the CHROMA.

The CHROMA is clocked and configured using a Xilinx Spartan-6 FPGA. The same FPGA also captures the data output from the ADCs and re-formats it to send to a computer via Camera Link. Due to limitations in our digital interfaces, we only digitize four of the eight available outputs from the CHROMA.

Laboratory Setup

We used the LiveView [3] software program developed at JPL to examine the Camera Link data in real time. This allows us to quickly optimize the FPA configuration and perform optical alignments. LiveView also allows us to record the data for offline processing.

The FPA is cooled with a cryocooler to a minimum temperature of 150 K, and its temperature is stabilized using a closed-loop heater and thermistor mounted to the FPA heatsink.

To measure the linearity, an InGaAs photodiode is mounted adjacent to the FPA. It is connected to a separate transimpedance amplifier to provide an independent measurement of the radiance at the FPA.

A shortpass filter with a cutoff wavelength of $1.67 \mu\text{m}$ placed in front of the FPA's optic so that the HgCdTe and InGaAs photodiode have similar spectral sensitivity. When the detector is cooled, this optical assembly reaches an equilibrium temperature of 210-220 K, acting as a cold shield. Together with the shortpass filter, little thermal emission from outside

the chamber should reach the FPA or InGaAs photodiode.

In order to build up the photon transfer curve, the FPA is stimulated with a flat field at various illumination levels. This is done by re-imaging the output of an integrating sphere onto the FPA. A quartz-tungsten-halogen (QTH) lamp is moved in and out of the input to the sphere using a remotely-controlled stage.

A USAF test pattern can also be placed in front of the integrating sphere. This creates high contrast and sharp edges in the image to allow us to measure crosstalk from output to output.

4. DATA

At each illumination level, we acquired images for 10 seconds across a range of pixel clock rates. These rates correspond to frame rates of 66.2, 99.3, and 149.1 Hz. In order to sample the same time duration, we used 667, 1000, and 1500 frames in the respective analysis for each frame rate, as summarized in Table 2. The FPA is operated in integrate-while-read (IWR) mode, so the integration time is 99% as long as frame period. In order to measure the electronic pedestal, we obtained images with nearly zero integration time by holding the pixel amplifier in reset for all but 1% of the readout time. Since these images are acquired with a different digital configuration than normal IWR operation, we do not use them to determine the read noise.

Out of 640x480 available pixels in each frame, we examine over 150,000, or 49%, of the pixels that are illuminated up to saturation and operating with a dark noise level below 500 e^- and dark current below 35000 e^- per frame.

Pixel Clock (MHz)	Frames per sec. (fps)	Frames Analyzed	Elect. Noise (DN)
5.56	66.2	667	3.62
8.33	99.3	1000	3.64
12.5	149.1	1500	3.98

Table 2: Pixel and frame rates used to characterize the CHROMA FPA. For the 3 frame rates tested, the number of frames in the timeseries is adjusted so that it covers 10 seconds in each case. The electronics noise is measured from the FPA output to the ADC.

5. ANALYSIS

Dark Current and Background

At each FPA temperature and frame rate tested, we measured the dark current and background from a set of frames with zero external illumination. We then subtracted off the electronic pedestal from the set of frames with nearly zero integration time.

Background thermal radiation also adds to the measured dark current. The front side of the FPA faces a cold shield with a temperature 216 K. If the cold shield radiates as a blackbody, then Planck’s Law integrates to $2.1 \times 10^4 e^- s^{-1} \text{pix}^{-1}$. This is a significant correction to the dark current measurement at 150 and 180 K.

Photon Transfer

We use the photon transfer method to determine the gain, read noise, and full well capacity of the FPA.

The gain is determined from the slope of the linear relationship between the variance (in units of DN^2) and the signal (in DN). Poisson (photon-counting) noise dominates in this region, whose variance (in units of e^-) is equal to the mean (in e^-), so the input-referred gain of e^-/DN can be determined.

With the electronic pedestal subtracted off, the read noise is equal to the y intercept of the photon transfer function. Due to the presence of dark current and its associated Poisson noise, the linear fit extrapolates the variance to zero signal.

The full well capacity can be defined by where the variance reaches its maximum value before collapsing at saturation. The maximum in the variance occurs at lower illumination values than where saturation affects the pixel values, so the variance is a more conservative estimate of the well capacity.

It is important to note how our application of the photon transfer method differs from the prescription in [2]:

First, we find the temporal variance of each pixel rather than the spatial variance across an image. Interpixel capacitance tends to reduce the spatial variance, making the spatial variance a poor estimate of the Poisson noise unless additional corrections are made.

Second, we fit a linear function to the photon transfer curve of each pixel, which reveals any gain variations from pixel to pixel. This also allows us to report the deviation in our measurements of read noise and well capacity. For speed, we use a simple least-squares regression.

Third, we estimate the noise using the absolute average deviation, rather than the standard deviation, for increased robustness against non-Gaussian noise. The goal is not to reduce the measured noise, but to increase the accuracy of the estimate in the face of external factors such as electronic interference or a dropped bit. We scale the absolute average deviation back up to the standard deviation by assuming a Gaussian distribution, for which the factor is $\sqrt{\pi/2}$ [4].

Finally, we note that the contributions to the variance from the electronics downstream of the FPA as well as the light source can depend on the signal level. If the read noise is not a constant term, it can skew the estimate of the photon transfer slope in either direction, and if the light source shows temporal variability, the shot noise might be overestimated as the signal increases.

The CHROMA FPA has a mode in which its analog outputs are connected to an internal digital-to-analog converter (DAC). By sweeping the DAC over the dynamic range of the output, we can determine any dependence of the electronics’ variance on the signal level. A linear fit to the variance across the dynamic range is subtracted from the measured variances, and it is shown as the “Electronics Correction” in the photon-transfer curves.

To address the instabilities in the light source, we can take a spatial mean of each image in the timeseries to minimize the Poisson noise. The variance in the resulting timeseries can then indicate the common-mode noise present in the image

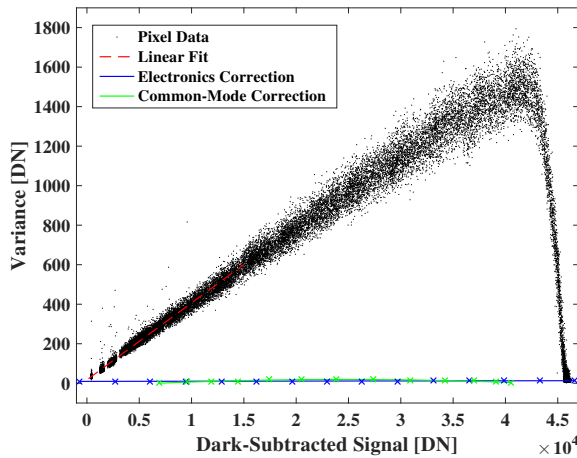


Figure 2: Photon transfer curve at 150 K and a 5.56 MHz pixel clock.

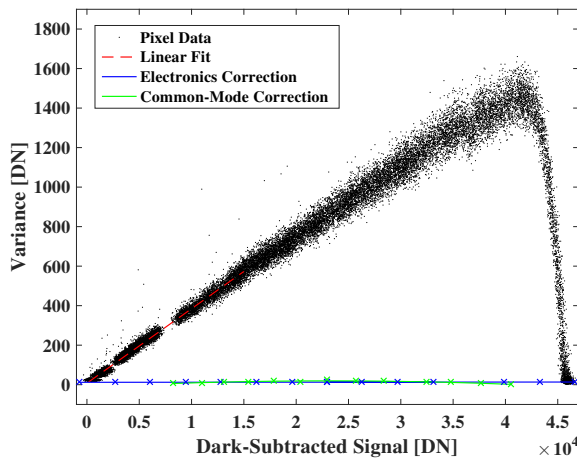


Figure 3: Photon transfer curve at 150 K and a 8.33 MHz pixel clock.

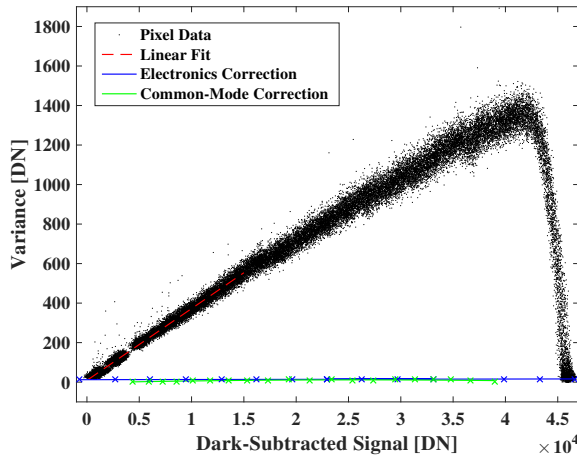


Figure 4: Photon transfer curve at 150 K and a 12.5 MHz pixel clock.

due to the illumination (or other sources, for that matter). It may be tempting to de-correlate the timeseries of the mean image from each pixel, but the two are not statistically independent, and structure in the illumination pattern from stray light could complicate the de-correlation.

Instead, the common-mode variance over signal is fitted with a second-order polynomial, and this function is subtracted from the measured variance. Although nonzero, this also turns out to be a very small correction, which we also plot as the “Common-Mode Correction” in the photon transfer curves.

Figures 2, 3, and 4 show the photon transfer curves resulting from this analysis. The measurements of signal and variance for each pixel and each illumination level are combined to make a single, nearly continuous curve. Some gaps exist for large changes in the illumination.

6. RESULTS AND DISCUSSION

Dark Current and Background

The dark current measured at 150 K, 180 K, and 200 K are reported in Table 3 for a 5.56 MHz pixel clock rates (66 frames per second). In addition, the contribution to the total noise from dark current is listed. Our dark current measurements at 150 K and 180 K are higher than those measured by the manufacturer for this particular device, but they are consistent for the value at 200 K. An additional source of thermal radiation in our test setup might impact the measurement at lower temperatures. The dark current measurements for this particular device are much higher those anticipated by the manufacturer from theoretical models of HgCdTe [1] as well as devices produced more recently. For our purposes, it is important to measure the dark current in order to arrive at the read noise.

Temp. (K)	Dark Current ($e^- s^{-1} \text{pix}^{-1}$)	Dark Noise, Expected ($e^- \text{pix}^{-1}$)	Dark+Read Noise, Meas. ($e^- \text{pix}^{-1}$)
150	$7.23 \pm 0.05 \times 10^5$	104	162 ± 15
180	$8.08 \pm 0.13 \times 10^5$	110	168 ± 15
200	$1.73 \pm 0.09 \times 10^6$	161	209 ± 138

Table 3: Measured dark current, equivalent dark noise, and measured total noise in a dark frame measured at 3 temperatures. A pixel clock of 5.56 MHz is used in all cases. The 216 K cold shield radiates a maximum of $2.1 \times 10^4 e^- s^{-1} \text{pix}^{-1}$, contributing 18 e^- to the dark noise.

Gain, Noise, Well Capacity

The three characteristics are readily determined from the photon transfer curve—the gain (in e^- / DN), the read noise, and the full well capacity—are summarized in Tables 4, 5, and 6. Due to the slight kink in some of the photon transfer curves near 2×10^4 DN, the linear fit is only performed up to 1.5×10^4 DN for each curve.

Here, the read noise is the constant term in the fit to the photon transfer curve. This is the appropriate value to use when modeling the FPA’s noise performance in normal IWR mode with the addition of Poisson noise from dark current and signal. The noise measured in the frames with minimized integration time is higher, but they do not represent normal

operation of the FPA. The total (read + dark current) noise in dark frames are reported in Table 3, which are indeed consistent with the quadrature sum of the read noise and dark noise.

The full well capacity is determined by finding the pixel value with the maximum variance for each photon transfer curve. This pixel value is multiplied by the gain to find the full well capacity.

The ratio of full well capacity to read noise gives the dynamic range, which is independent of the conversion gain. At a pixel clock rate of 8.33 MHz, the dynamic range is consistent with the value of 9090 in [1]. However, it is slightly lower at pixel clock rates of 5.56 MHz or 12.5 MHz. While one should expect the noise at 12.5 MHz to be higher due to the signal not being as settled, the higher noise at 5.56 MHz is unexpected. The bias and timing registers for the FPA might have to be re-optimized for a lower pixel clock rate; they were held constant from 5.56 MHz to 12.5 MHz here. Alternatively, the longer pixel period could admit higher noise if $1/f$ noise is present in the pixel amplifier or sample-and-hold circuits.

Linearity

We assess the linearity by comparing the output of the CHROMA FPA to an independent InGaAs photodiode, shown in the top panel of Figure 5. The cross-comparison agrees to a linear fit to within $\pm 2\%$ for much of the dynamic range of the CHROMA, shown in the bottom panel of Figure 5. The scatter in the nonlinearity at low signal levels could be partly due to inaccuracies in measuring the InGaAs photocurrent.

Pixel Clock (MHz)	Gain (e^-/DN)	Read Noise (e^-)	Full Well (Me^-)
5.56	25.3 ± 1.3	129 ± 29	1.015 ± 0.077
8.33	25.8 ± 1.1	108 ± 46	1.040 ± 0.070
12.5	26.9 ± 0.8	120 ± 47	1.095 ± 0.053

Table 4: Gain, read noise, and well capacity computed from linear fits to the photon transfer curves at 150 K.

Pixel Clock (MHz)	Gain (e^-/DN)	Read Noise (e^-)	Full Well (Me^-)
5.56	25.0 ± 1.4	121 ± 32	0.995 ± 0.076
8.33	26.2 ± 0.97	116 ± 23	1.058 ± 0.059
12.5	27.3 ± 1.0	123 ± 24	1.097 ± 0.060

Table 5: Gain, read noise, and well capacity computed from linear fits to the photon transfer curves at 180 K.

Pixel Clock (MHz)	Gain (e^-/DN)	Read Noise (e^-)	Full Well (Me^-)
5.56	25.0	134	0.990
8.33	26.0 ± 3.8	114 ± 86	1.041 ± 0.157
12.5	27.1 ± 1.1	137 ± 31	1.084 ± 0.065

Table 6: Gain, read noise, and well capacity computed from linear fits to the photon transfer curves at 200 K. A wide scatter in the gain measurements at 5.56 MHz make the standard deviation unreliable; only the median value is listed.

Power Dissipation

Infrared photodiode FPAs, including HgCdTe, must be cooled to reduce their dark current to usable levels; hence, it is important to know the power dissipation of the FPA to design its cooling system. The power measurements are summarized in Table 7. As expected, the power dissipation rises with the pixel clock rate. Since DAC settings in the FPA have a large impact on the power dissipation, it may be possible to reduce the dissipation with optimized DAC settings. Our measurements are generally consistent with the 150 mW quoted by the manufacturer with a 10 MHz pixel clock [1].

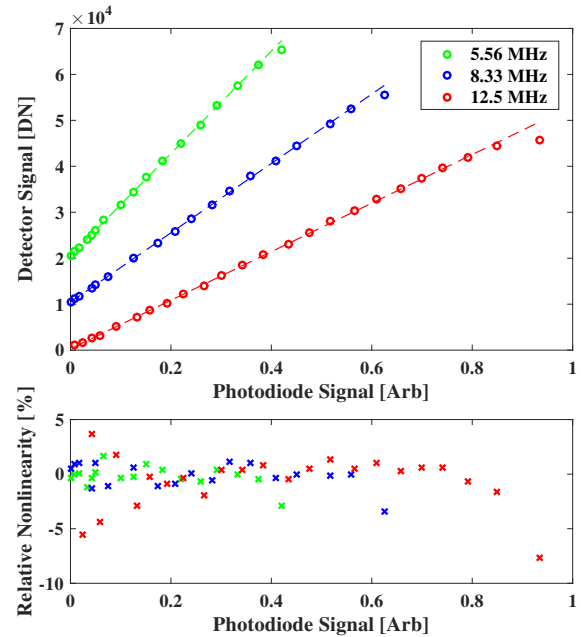


Figure 5: Top: Linearity of the CHROMA FPA at 150 K, spaced by 10^4 DN for clarity, measured against a reference photodiode. Bottom: Residuals from the linear fit (shown as a dashed line in the top panel) show $\pm 2\%$ nonlinearity for much of the dynamic range.

Pixel Clock (MHz)	Power at 150K (mW)	Power at 180K (mW)	Power at 200K (mW)
5.56	152	142	137
8.33	158	149	145
12.5	178	168	165

Table 7: Power dissipation measured as a function of frame rate and operating temperature. The detector is dark, which maximizes the power consumption.

Crosstalk

Each CHROMA FPA is built up from panels that are 160 pixels wide and 480 pixels tall; the 1280-by-480 device stitches eight such panels. Having multiple outputs is key to achieving a high frame rate while still allowing the analog output to settle. However, it also opens a path for crosstalk between the outputs.

We measured the crosstalk by imaging the vertical bars of a USAF test pattern onto the FPA, shown in Figure 6. The

bars were illuminated nearly to saturation, and the rest of the FPA was dark (with the exception of stray light). The pixel clock is 12.5 MHz in this test since higher pixel rates are more susceptible to crosstalk.

We calculated the median of the illuminated rows, and then we split the mean row into the 4 panels, which contain 160 columns each. For the two illuminated panels, the bars are clearly visible from 1.5×10^4 to 5.5×10^4 DN, as seen in Figure 7.

For the two non-illuminated panels, we do not see a correlation with the illuminated columns, even after removing a third-order polynomial from the dark columns. Therefore, a cross-correlation is necessary to quantify the crosstalk, or at least place an upper bound on it. We define the crosstalk to be

$$-20 \log_{10} \frac{E[(x - \bar{x})(y - \bar{y})]}{\sigma_x^2} \quad (1)$$

where x denotes the illuminated signal, and y denotes the dark signal, and E denotes the expectation (mean) operator. By offsetting x with respect to y , the numerator becomes a cross-correlation, and the denominator normalizes it.

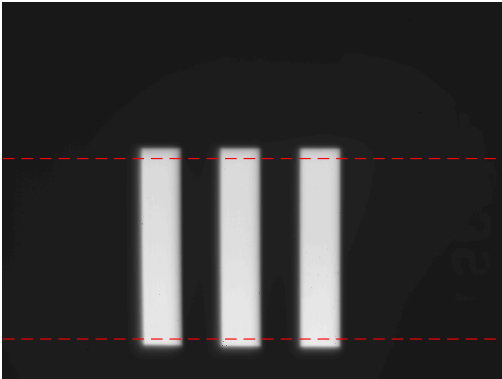


Figure 6: For the crosstalk measurement, the vertical bars from a USAF test target are re-imaged onto the FPA. The rows between the red dashed lines are averaged in the subsequent analysis.

The bottom panel of Figure 7 shows the results of this computation. The crosstalk to output 1 from outputs 2 and 3 peaks at -71 dB, and the crosstalk to output 4 from outputs 2 and 3 peaks at -69 dB. However, the lack of a strong peak at zero offset indicates that the apparent correlations could be due to structure in the dark signals that are unrelated to the sharp edges in the illuminated pattern. Therefore, the mean crosstalk of -70 dB should be interpreted as an upper bound. Additional testing of the analog signal chain alone could better isolate any sources of crosstalk.

7. CONCLUSIONS AND FUTURE WORK

We have found that the CHROMA FPA has well-behaved read noise and full well capacity across more than an octave of pixel clock rates and temperatures from 150 to 200 K. Measurements with the entire signal chain indicate that the crosstalk is at or below -70 dB. The dynamic range is at or above 79 dB at a pixel clock rate of 8.33 MHz. The dynamic

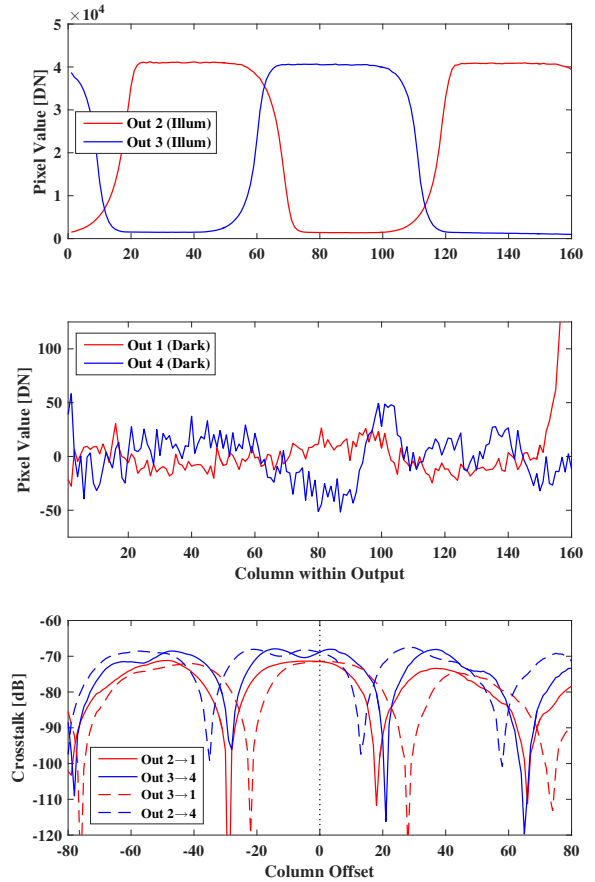


Figure 7: *Top Panel*—The row-wise median values of each output are plotted to show the columns that are read out simultaneously. Vertical bars are imaged onto the portion of the FPA feeding outputs 2 and 3. *Middle Panel*—We look for crosstalk to outputs 1 and 4. *Bottom Panel*—A cross-correlation shows the crosstalk to be approximately -70dB or lower since there is no discernible peak in the cross-correlation at zero column offset.

range and the power consumption are consistent values we expect from the manufacturer [1], although the dark current of this particular device remains higher than expected.

The CHROMA FPA also shows high resilience to radiation, but some degradation remains permanent for specific pixels. We will soon characterize HgCdTe CHROMA FPAs integrated into imaging spectrometers, which will allow us to characterize the spectral response and re-examine the dark current. These FPAs will be further tuned to maximize the dynamic range and minimize the power consumption for the clock frequencies at which they will operate.

ACKNOWLEDGMENTS

This research was carried out at the Jet Propulsion Laboratory, California Institute of Technology, under a contract with the National Aeronautics and Space Administration. The authors wish to thank Emily Brageot, Daniel Preston, Jaime Luna, Heather Owen, Antonio Fonseca, John Shaw, and Marco Hernandez for their help with building various aspects of the test setup.

REFERENCES

- [1] R. T. Demers, J. W. Bailey, Robert a d Beletic, S. Bernd, S. Bhargava, J. Herring, P. Kobrin, D. Lee, J. Pan, A. Petersen, E. Piquette, B. Starr, M. Yamamoto, and M. Zandian, "The chroma focal plane array: a large-format, low-noise detector optimized for imaging spectroscopy," in *Proceedings of the SPIE*, 201, p. 88700J.
- [2] J. R. Janesick, *Photon Transfer*. SPIE Publications, 2007.
- [3] "Liveview: A new utility for real-time calibration of focal plane arrays using commodity hardware," in *2016 IEEE Aerospace Conference*. IEEE, 2016, pp. 1–8.
- [4] R. Geary, "The ratio of the mean deviation to the standard deviation as a test of normality," *Biometrika*, pp. 310–332, 1935.
- [5] B. S. Richardson, M. L. Eastwood, C. F. Bruce, R. O. Green, and J. Coles, "Mercury-cadmium-telluride focal plane array performance under non-standard operating conditions," in *2011 IEEE Aerospace Conference*. IEEE, 2011, pp. 1–6.
- [6] J. Pan, "Teledyne imaging sensors chroma visible-infrared focal plane array," *Teledyne Imaging Sensors, Inc*, 2012.



Peter Sullivan is an electrical engineer specializing in mixed-signal design and infrared instrumentation at the NASA Jet Propulsion Laboratory. He has previously worked at the Johns Hopkins Applied Physics Laboratory and holds a B.S. from Cornell University and a S.M. from the Massachusetts Institute of Technology. He has characterized image sensors for applications ranging from

Earth science to exoplanet detection.



Michael Bernas is an electrical engineer specializing in mixed-signal design for FPA applications related to imaging spectroscopy at the NASA Jet Propulsion Laboratory. He holds a B.S. from University of California, Santa Barbara and a M.S. from the University of Southern California. He has previously worked on a 5 megapixel IR camera at Lockheed Martin Santa Barbara Focalplane.



Elliott Liggett is an Analog Circuits and DSP engineer specializing in Imaging Spectroscopy applications at the Jet Propulsion Laboratory. An active ham radio operator since he was a teenager, Elliott has an extensive background in hands-on analog design. Before receiving his bachelors in EE at the University of Arizona in 2012, he designed equipment and software in the music production industry. At the University of Arizona, he worked under Dr. Chris Walker in the Steward Observatory Radio Astronomy Lab on SuperCam, a 64-pixel superconductor THz receiver.